SHORT-WAVELENGTH ELECTROSTATIC FLUCTUATIONS IN THE SOLAR WIND

F. VALENTINI, D. PERRONE, AND P. VELTRI

Dipartimento di Fisica and CNISM, Università della Calabria, 87036 Rende (CS), Italy

ABSTRACT

Hybrid Vlasov–Maxwell simulations have been used recently to investigate the dynamics of the solar-wind plasma in the tail at short wavelengths of the energy cascade. These simulations have shown that a significant level of electrostatic activity is detected at wavelengths smaller than the proton inertial scale in the longitudinal direction with respect to the ambient magnetic field. In this paper, we describe the results of a new series of hybrid Vlasov–Maxwell simulations that allow us to investigate in more detail the generation process of these electrostatic fluctuations in terms of the electron-to-proton temperature ratio T_e/T_p. This analysis gives evidence for the first time that even in the case of cold electrons, $T_e \simeq T_p$ (the appropriate condition for solar-wind plasmas), the resonant interaction of protons with large-scale left-hand polarized ion-cyclotron waves is responsible for the excitation of short-scale electrostatic fluctuations with an acoustic dispersion relation. Moreover, through our numerical results we propose a physical mechanism to explain the generation of longitudinal proton-beam distributions in typical conditions of the solar-wind environment.

Key words: plasmas – turbulence – waves

Online-only material: color figures

1. INTRODUCTION

The study of the short-wavelength region of the solar-wind turbulent cascade represents a subject of recent active interest in space plasma physics. Many experimental works (Bale et al. 2005; Sahraoui et al. 2009; Alexandrova et al. 2009) have focused on the analysis of the solar-wind data from spacecraft, aiming to investigate how the energy of large-scale Alfvénic fluctuations can be transferred toward short scales and eventually turned into heat. Within this scenario a crucial point is the identification of the fluctuations that channel the energy from large to short wavelengths along the turbulent cascade.

Matthaeus et al. (1986) showed that in the solar wind the magnetohydrodynamic fluctuations are comprised mainly of two populations: the first one with wavevectors predominantly perpendicular to the ambient magnetic field (two-dimensional (2D) turbulence) and the second one with wavevectors aligned to the background field (slab turbulence). As recently discussed, for example, by means of gyrokinetic simulations (Howes et al. 2008), 2D turbulence seems to give rise to, at length, scales below the ion-gyro scale to transverse electromagnetic fluctuations whose features are consistent with so-called kinetic Alfvén waves. These results provide a significant interpretation to solar-wind observations from the *Cluster* spacecraft (Sahraoui et al. 2009) in which a quasi-2D cascade into kinetic Alfvén waves seems to be identified. This cascade represents, then, a channel available to bring energy from large to small scales.

The second population (slab turbulence) can produce a second channel, in the form of electrostatic fluctuations, for the transportation of energy toward small scales. The first insight into the nature of this kind of phenomenon date back to the late 1970s, when solar-wind measurements from the *Helios* spacecraft (Gurnett & Anderson 1977; Gurnett & Frank 1978; Gurnett et al. 1979) showed that the high-frequency (a few kHz) range of the solar-wind turbulent cascade is characterized by the presence of a significant level of electrostatic activity identified as ion-acoustic (IA) waves propagating parallel to the ambient magnetic field. The energy level of these fluctuations

shows a certain correlation with the electron-to-proton temperature ratio T_e/T_p and surprisingly survives even for small values of T_e/T_p, for which linear Vlasov theory (Krall & Trivelpiece 1986) predicts strong Landau dissipation. The propagation of these fluctuations seems to be correlated with the generation of non-Maxwellian proton velocity distributions that display the presence of beams of accelerated particles in the direction of the ambient magnetic field, moving with mean velocity close to the local Alfvén speed. More recent data from the *WIND* (Mangeney et al. 1999; Lacombe et al. 2002) and the *Cluster* (Pickett et al. 2004) spacecraft has allowed more detailed analysis of the features of this electrostatic activity at high frequency in the solar wind. Subsequent experimental space observations confirmed that the particle velocity distributions show a general tendency to depart from the Maxwellian equilibrium configuration, displaying temperature anisotropy (Holloweg & Isenberg 2002; Marsch et al. 2004; Hellinger at al. 2006) and generating field-aligned accelerated beams (Marsch et al. 1982; Tu et al. 2004; Heuer & Marsch 2007).

These experimental results support the idea that kinetic effects are at work in the solar-wind plasmas at short spatial scale lengths, but many aspects of the experimental evidence discussed above still need a convincing physical interpretation: (1) how electrostatic fluctuations of the IA type can survive against damping in the case of cold electrons ($T_e \simeq T_p$) and (2) why the mean velocity of the field-aligned beam of accelerated protons is commonly observed to be of the order of the local Alfvén speed.

Recently, many authors have used kinetic numerical simulations to reproduce the solar-wind phenomenon described above, that is, the generation of longitudinal proton-beam velocity distributions associated with the propagation of electrostatic fluctuations. In particular, Araneda et al. (2008) presented one-dimensional (1D) hybrid particle-in-cell (PIC) simulations in which IA fluctuations, generated through parametric instability of monochromatic Alfvén-cyclotron waves, produced field-aligned proton beams during the saturation phase of the wave–particle interaction process. More recently, Matteini

et al. (2010) analyzed in detail the relationship between the kinetic aspects of the parametric instability of Alfvén waves (in the case of monochromatic pump waves and of a spectrum of waves) and the evolution of the proton distribution functions, again making use of numerical PIC simulations in a hybrid regime.

The parametric instability of left-handed polarized Alfvén waves, considered in the papers referenced above, is efficient at producing IA fluctuations in regimes of low values of the proton plasma beta β_p (Longtin & Sonnerup 1986) and for large values of the electron-to-proton temperature ratio, since IA waves are heavily Landau-damped for small T_e/T_p (Krall & Trivelpiece 1986). From the solar-wind observations, the mean velocity of the longitudinal proton beam is typically of the order of the local Alfvén speed. As discussed by Araneda et al. (2008) and Matteini et al. (2010), the IA fluctuations, produced through parametric instability, trap resonant protons and dig the particle velocity distribution in the vicinity of the wave phase speed, thus creating a field-aligned beam; it follows that, in order to generate a beam with a mean velocity close to V_A through this mechanism, the phase velocity $v_\phi^{(IA)}$ of the IA fluctuations must be of the same order of V_A ($v_\phi^{(IA)} \simeq V_A$). Taking into account that the phase speed of the IA waves is $v_\phi^{(IA)} \simeq \sqrt{T_e/m_p}$, the condition necessary to produce a beam with mean velocity of the order of V_A is $T_e/m_p \simeq V_A^2 \Rightarrow T_e/T_p \simeq m_p V_A^2/T_p \simeq 1/\beta_p$, or, equivalently, $(T_e/T_p)\beta_p \simeq 1$. Large values of T_e/T_p, needed for IA fluctuations to survive against Landau damping, require low values of β_p to keep this condition valid. This range of parameters is unusual for the solar-wind plasma, where the electron-to-proton temperature ratio varies in the range $0.5 < T_e/T_p < 4$ (Schwenn & Marsch 1991), while β_p is typically of order unity. Moreover, it is not clear why the electrostatic activity in the high-frequency region of the solar-wind energy spectra is observed even at low values of T_e/T_p and why the secondary proton beam always has a mean velocity of the order of the local Alfvén speed.

Besides the numerical simulations described above, a newly developed Eulerian hybrid Vlasov–Maxwell code (Valentini et al. 2007) has been used to propose a different mechanism for the generation of proton-beam distributions associated with short-scale electrostatic activity in the solar wind. This code numerically solves the Vlasov equation for the protons, while the electrons are considered a fluid; a generalized Ohm's equation for the electric field, where the Hall term and the electron inertia terms are retained, is integrated. The Faraday equation, the equation for the curl of the magnetic field (where the displacement current is neglected), and an isothermal equation of state for the electron pressure round out the set of equations. The quasi-neutrality assumption is considered.

These hybrid Vlasov–Maxwell simulations in 1D–3V phase-space configuration (one dimension in physical space and three dimensions in velocity space; Valentini et al. 2008; Valentini & Veltri 2009) were focused on a physical situation where magnetohydrodynamic turbulence evolves to a state where a significant amount of energy is stored in longitudinal wavevector modes (slab turbulence; Dobrowolny et al. 1980; Matthaeus et al. 1986; Carbone et al. 1995). The turbulent energy cascade is triggered by nonlinear wave–wave interactions of large-scale ion-cyclotron (IC) waves. The numerical results from these simulations give evidence that for large values of the electron-to-proton temperature ratio ($T_e/T_p = 10$) the tail of the turbulent cascade at short scales is characterized by the presence

of electrostatic fluctuations, propagating in the direction of the mean magnetic field. The Fourier $k - \omega$ spectrum of the numerical signals reveals that, in addition to the IA branch, a new branch of waves appears with phase speeds close to the proton thermal speed and with an acoustic dispersion relation. These new waves have been dubbed ion-bulk (IBk) waves. It has been shown that diffusive plateaus, created in the longitudinal proton velocity distribution through resonant interactions of protons with IC waves (Kennel & Engelmann 1966; Heuer & Marsch 2007), are responsible for the excitation of the IBk waves. This phenomenon leads to the generation of a beam of accelerated protons in the direction of the ambient field with a mean velocity close to V_A. These results have been confirmed through hybrid-Vlasov simulations in 2D–3V phase-space configuration (Valentini et al. 2010). Moreover, in 2011 (Valentini et al. 2011) the existence of the IBk waves has also been demonstrated by means of electrostatic kinetic simulations in which an external driver electric field is used to create a longitudinal plateau in the proton velocity distribution.

In the present paper, we discuss the results of a new series of 1D–3V hybrid Vlasov–Maxwell simulations (in physical situations of slab turbulence) in which the development of the turbulent cascade toward short spatial lengths is investigated in terms of the electron-to-proton temperature ratio. This analysis allows us to demonstrate that the electrostatic fluctuations at short wavelengths, generated as the result of the turbulent cascade, can last in typical conditions of the solar-wind plasma, that is, even for low values of T_e/T_p. Moreover, through our numerical simulations we describe a physical mechanism leading to the generation of a field-aligned proton beam with mean velocity close to the Alfvén speed that works even for small values of T_e/T_p provided the proton plasma beta is of order unity.

2. NUMERICAL RESULTS

As discussed in the Introduction, we numerically follow the kinetic dynamics of protons in 1D–3V phase-space configuration (periodic boundary conditions are imposed in physical space). In the following, times are scaled by the proton cyclotron frequency Ω_{cp}, velocities by the Alfvén speed $V_A = B_0/\sqrt{4\pi\rho}$ (B_0 being the magnetic field and ρ the mass density), lengths by the proton skin depth $\lambda_p = V_A/\Omega_{cp}$, and masses by the proton mass m_p.

We assume that at $t = 0$ the plasma has uniform density and is embedded in a background magnetic field $\mathbf{B}_0 = B_0\mathbf{e}_x$, with a superposed set of Alfvén waves circularly left-hand polarized in the plane perpendicular to the mean magnetic field and propagating along it. The explicit expressions for the velocity and magnetic perturbations ($\delta u_y(x), \delta u_z(x), \delta B_y(x), \text{and } \delta B_z(x)$) were derived from the linearized two-fluid equations (Valentini et al. 2007). The first three modes in the spectrum of velocity and magnetic perturbations are excited at $t = 0$ in such a way that the maximum perturbation amplitude is $A = 0.5$. No density disturbances are imposed at $t = 0$. The initial Maxwellian ion distribution is $f(x, \mathbf{v}, t = 0) = A(x) \exp(-(\mathbf{v} - \delta\mathbf{u})^2/\beta_p)$, where $\beta_p = 2v_{tp}^2/V_A^2$ ($v_{tp} = \sqrt{T_p/m_p}$ is the proton thermal speed and T_p the proton temperature); $A(x)$ is such that the velocity integral of f gives an equilibrium density of $n_0 = 1$. The value of the proton plasma beta is fixed at $\beta_p = 0.5$ (the proton thermal velocity is $v_{tp} = 0.5$) and the system evolution is analyzed for different values of the electron-to-proton temperature ratio ($T_e/T_p = 1, 3, 6, \text{and } 10$). The mass ratio is $m_e/m_p = 1/1836$.

The length of the physical domain is $L_x \simeq 40.2$ (the fundamental wavenumber is $k_1 = 2\pi/L_x \simeq 0.156$), while the limits of the velocity domain in each direction are fixed at $v^{\max} = 5v_{\mathrm{tp}}$. We use 2048 gridpoints in physical space, 51^3 in velocity space, and a time step of $\Delta t = 10^{-3}$. The simulation is carried up to $t = 400$.

The nonlinear three-wave interactions at large scales trigger the turbulent energy cascade. When the energy is carried at frequencies close to Ω_{cp}, the resonant interaction of the protons with the IC waves produces the formation of a diffusive plateau in the longitudinal velocity distribution in the vicinity of the phase speed $v_\phi^{(\mathrm{IC})}$ of the IC waves (Valentini et al. 2008). For parallel propagating IC waves one has $v_\phi^{(\mathrm{IC})} \simeq V_A$ for frequencies smaller than Ω_{cp} (or equivalently for small wavenumbers) and $v_\phi^{(\mathrm{IC})} < V_A$ for frequencies close to Ω_{cp}. If β_p is of order unity one gets $v_\phi^{(\mathrm{IC})} \lesssim V_A \simeq v_{\mathrm{tp}}$; this means that the diffusive plateau is created in the vicinity of the proton thermal speed, or, equivalently, in the bulk of the proton velocity distribution.

When the proton velocity distribution is flattened in the vicinity of v_{tp}, the IBk waves can be excited (Valentini et al. 2008, 2011; Valentini & Veltri 2009) and the energy is transferred from large to short wavelengths along the IBk channel. From the analysis of the numerical results, one realizes that in the range of large wavenumbers, say $k > 10\lambda_p^{-1}$, the parallel electric energy is the dominant component of the energy spectrum, meaning that the tail at short wavelengths of the turbulent cascade is characterized by the presence of electrostatic activity. In the top panel of Figure 1, we report in a semi-logarithmic plot the early time evolution $(0 < t < 100)$ of the longitudinal electric energy at small scales evaluated as $\mathcal{E}(t) = \sum_k |E_{k_x}|^2$ with $k > 10\lambda_p^{-1}$. The black line (1) corresponds to a simulation with $T_e/T_p = 10$, the red line (2) to $T_e/T_p = 6$, the blue line (3) to $T_e/T_p = 3$, and the green line (4) to $T_e/T_p = 1$. It is clear from this figure that, during the system evolution, $\mathcal{E}$ displays a sudden exponential growth and then a saturation phase. We note that for $T_e/T_p = 1$ the exponential growth phase is somewhat delayed with respect to the cases with $T_e/T_p = 10, 6$, and 3.

The physical mechanism responsible for this exponential growth consists of an instability process of the beam-plasma type (Valentini et al. 2011): the resonant interaction of protons with IC waves of large amplitude creates regions of positive slope (small bumps) instead of flat plateaus in the longitudinal proton velocity distribution at v_{tp}; this triggers the growth of high wavenumbers' electric field components in parallel propagation with phase speed comparable to v_{tp}. As recently shown by Valentini et al. (2011), the IBk waves can be excited only when a plateau in the longitudinal proton velocity distribution is generated in the vicinity of v_{tp}. In the present hybrid Vlasov–Maxwell simulations, a diffusive longitudinal plateau is generated at $v_\phi^{(\mathrm{IC})} \lesssim V_A$ as the result of the resonant interaction between IC waves and protons; when β_p is of order unity one gets $v_\phi^{(\mathrm{IC})} \lesssim V_A \simeq v_{\mathrm{tp}}$, meaning that a plateau can be produced at v_{tp} and the IBk waves can be excited. We considered different simulations with $0.5 \leqslant \beta_p \leqslant 2$ and obtained the same qualitative system evolution. On the other hand, the mechanism described above cannot work for small values of β_p.

The growth of $\mathcal{E}$ corresponds to the excitation of electrostatic fluctuations at high wavenumbers. The energetic level of these fluctuations after the saturation of the exponential growth depends on T_e/T_p; the largest saturation value of $\mathcal{E}$ is found
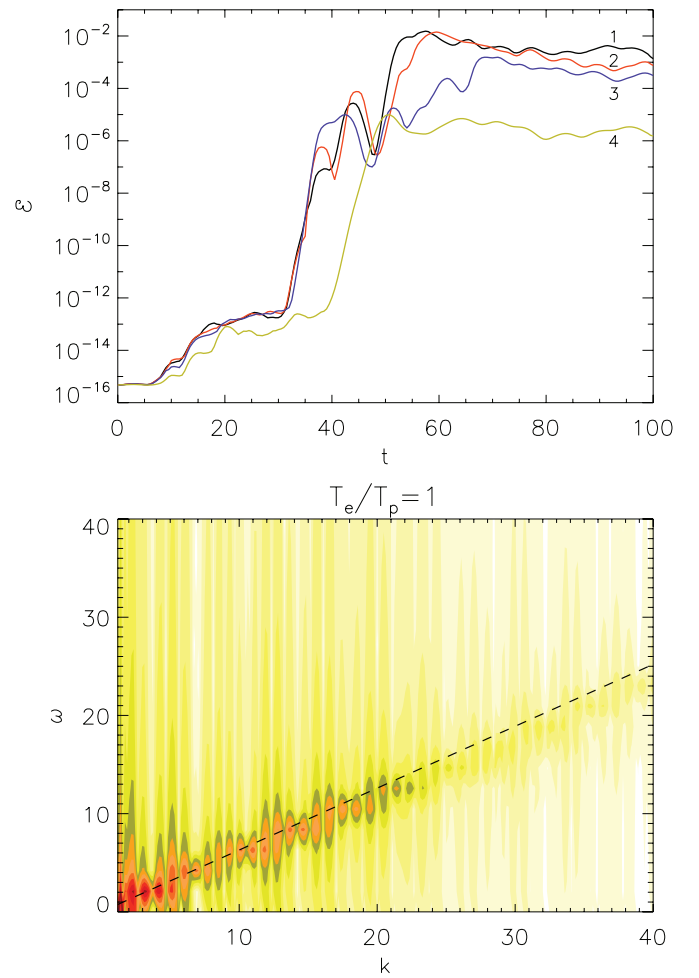

Figure 1. Top panel: time evolution of $\mathcal{E}$ for $T_e/T_p = 10$ (black line (1)), $T_e/T_p = 6$ (red line (2)), $T_e/T_p = 3$ (blue line (3)), and $T_e/T_p = 1$ (green line (4)); bottom panel: $k - \omega$ spectrum of the parallel electric energy for the case of $T_e/T_p = 1$.

(A color version of this figure is available in the online journal.)

for $T_e/T_p = 10$, but even at $T_e/T_p = 1$ a significant level of fluctuations is recovered. In the bottom panel of Figure 1, we show the $k - \omega$ spectrum of the parallel electric energy for the simulation with $T_e/T_p = 1$. The acoustic branch visible in this spectrum is the branch of IBk waves with a phase speed $v_\phi^{(\mathrm{IBk})} \sim 1.2 v_{\mathrm{tp}}$ (black dashed line). As shown by Valentini et al. (2008) and Valentini & Veltri (2009), for a simulation with $T_e/T_p = 10$ the branch of IA waves also appears in the $k - \omega$ spectrum of the parallel electric energy beside the IBk branch. For such a large value of T_e/T_p, the IA fluctuations generated in the early stage of the system evolution by ponderomotive effects can survive against Landau damping up to the end of the simulation. Nevertheless, here we show that when decreasing the value of T_e/T_p these IA waves are Landau-damped quite soon and disappear from the $k - \omega$ spectrum, as is clear from the bottom panel of Figure 1 for $T_e/T_p = 1$.

In the top panel of Figure 2, we show the electric field E_x as a function of x at the end of the simulation for the case $T_e/T_p = 3$. As can be clearly seen in this plot, a short-scale localized wave packet is generated as the results of the phenomenon described above. We point out that for simulations with $T_e/T_p = 1, 6$, and 10, we observed the generation of similar structures with amplitudes that depend on T_e/T_p (the largest amplitude is found for $T_e/T_p = 10$). These electrostatic
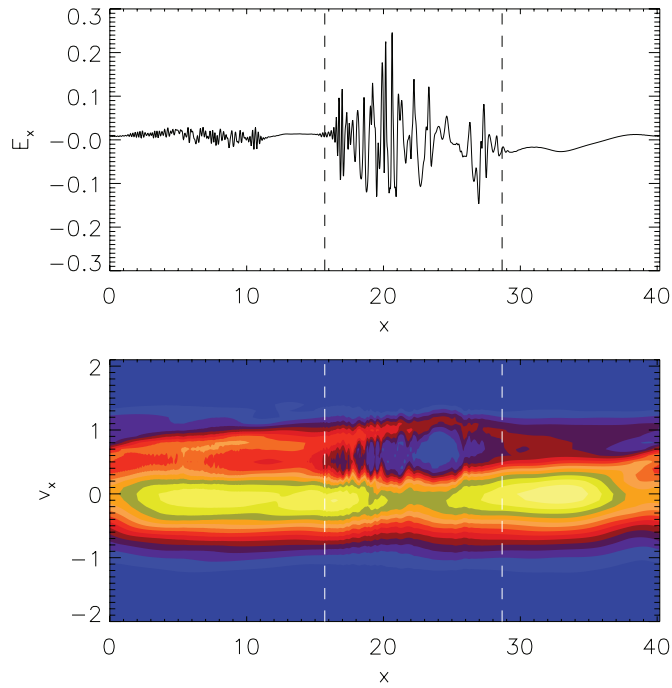
Figure 2. Top panel: parallel electric field E_x vs. x at $t = 100$; bottom panel: longitudinal phase-space level lines of the proton distribution function at $t = 100$.

(A color version of this figure is available in the online journal.)

Figure 4. Time evolution of $\mathcal{E}$ for a simulation with $T_e/T_p = 10$, for $A = 0.5$ (black line (1)) and $A = 0.2$ (red line (2)).

(A color version of this figure is available in the online journal.)

signals propagate with phase velocity $v_\phi \simeq v_{\mathrm{tp}}$ (independent of T_e/T_p) and trap resonant protons moving with a velocity close to v_{tp}. This is shown in the bottom panel of Figure 2, where the contour lines of the longitudinal phase-space proton distribution function are represented at $t = 100$ for $T_e/T_p = 3$; the region of trapped particles is delimited in space by the vertical white dashed lines and moves with a mean velocity close to $v_{\mathrm{tp}} = 0.5$.

In order to show how the generation of a trapped particle population affects the proton velocity distribution, in Figure 3 we report the v_x–v_y level curves of f, integrated over v_z and averaged over x in the interval corresponding to the trapping region (see the white dashed lines at the bottom in Figure 2), for $T_e/T_p = 1$ (a), $T_e/T_p = 3$ (b), $T_e/T_p = 6$ (c), and $T_e/T_p = 10$ (d), at $t = 100$. In each plot of Figure 3 a beam of accelerated protons is generated in the direction of the ambient magnetic field. We point out that the mean velocity of this secondary beam (of the order of $V_A = 1$), as well as its height, is independent of the value of T_e/T_p. We emphasize that this numerical evidence provides a reliable interpretation of the physical mechanism
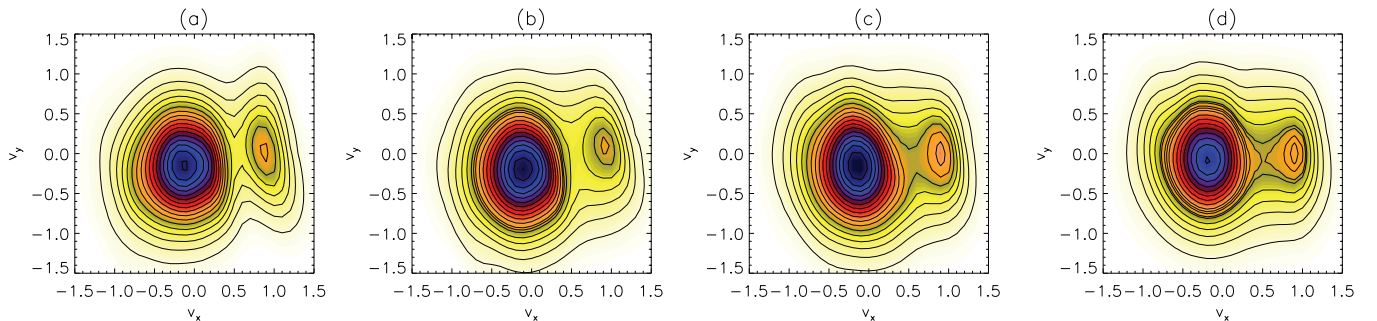
leading to the generation of field-aligned beams of protons in the solar-wind velocity distributions.

As a next step, we consider a new simulation with $T_e/T_p = 10$ in which we decrease the amplitude of the initial Alfvénic perturbations to the value $A = 0.2$ and compare the results of this new simulation with those of the old simulation with $A = 0.5$. In Figure 4, we report the time evolution of $\mathcal{E}$ (as defined above) for the case with $A = 0.5$ (black line (1)) and $A = 0.2$ (red line (2)) up to $t = 160$. We point out that decreasing the amplitude of the initial perturbations corresponds to a delay in the exponential growth of the electrostatic fluctuations at small scales and also to a decrease of the growth rate of $\mathcal{E}$. Moreover, the saturation level of $\mathcal{E}$ is about two orders of magnitude lower for $A = 0.2$ with respect to $A = 0.5$. Except for the differences discussed above, Figure 4 would suggest that the system dynamics are qualitatively similar for both cases $A = 0.2$ and $A = 0.5$; nevertheless, analyzing the numerical results in more detail, we realized that this is not true.

In Figure 5, we show the $k - \omega$ spectra of the longitudinal electric energy for the two simulations with $T_e/T_p = 10$ and $A = 0.5$ (a) and $A = 0.2$ (b). As already shown by Valentini et al. (2008), for $A = 0.5$ we distinguish two different branches of acoustic waves, the IA waves (upper branch) and the IBk waves (lower branch). The upper dashed line in the top panel of Figure 5 represents the theoretical prediction for the ion-sound speed c_s (Krall & Trivelpiece 1986), while the lower dashed line

Figure 3. v_x–v_y contour lines of the proton distribution function integrated over v_z and averaged over x in the region corresponding to the trapped particle population, for $T_e/T_p = 1$ (a), $T_e/T_p = 3$ (b), $T_e/T_p = 6$ (c), and $T_e/T_p = 10$ (d).

(A color version of this figure is available in the online journal.)
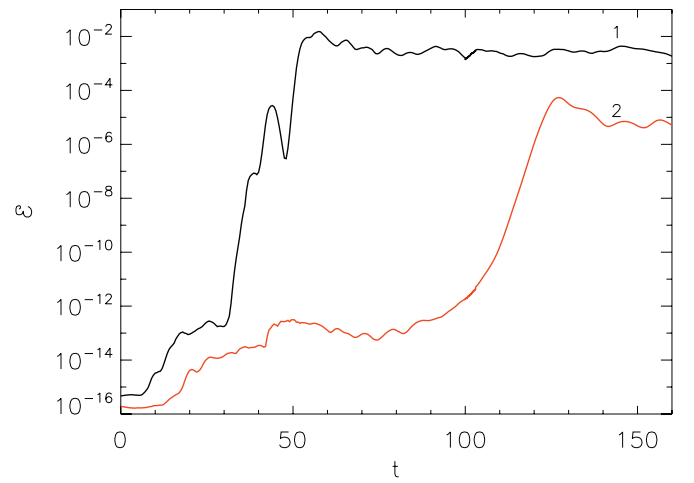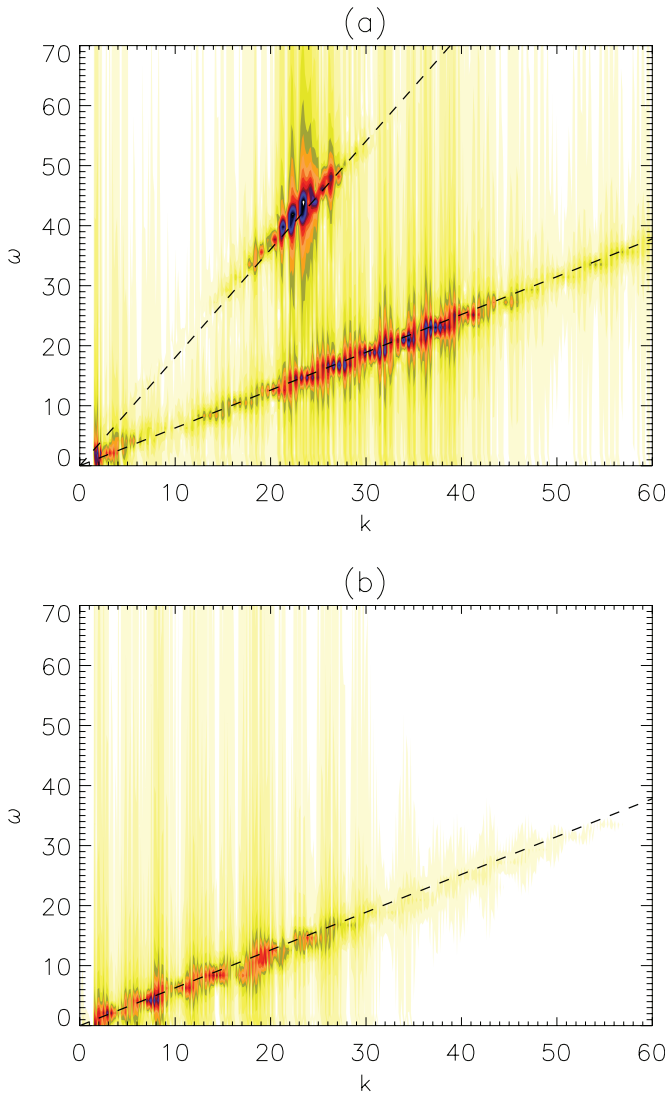
Figure 5. $k - \omega$ spectrum of the parallel electric energy for a simulation with $T_e/T_p = 10$, for $A = 0.5$ (a) and $A = 0.2$ (b).

(A color version of this figure is available in the online journal.)

represents the IBk waves' phase speed $v_\phi^{(\mathrm{IBk})} \sim 1.2 v_{\mathrm{tp}}$. As we discussed earlier, the IA waves are produced by ponderomotive effects. On the other hand, it is clear from the bottom panel of Figure 5 that, when decreasing the amplitude of the initial perturbations to the value $A = 0.2$, the branch of the IA waves disappears. This is due to the fact that decreasing the amplitude of the perturbation produces a decrease in the density fluctuations generated through ponderomotive effects, thus making the IA fluctuations too weak to survive against Landau damping.

The numerical results shown in Figure 5 allow us to conclude that the IBk waves represent the main component of the longitudinal electric energy spectrum at short scales. The IA waves can represent an additional ingredient when the amplitude of the perturbations is large enough to allow ponderomotive effects to produce high-level density fluctuations, but they disappear in the weak perturbation limit.

Finally, we analyze the features of the system dynamics at late times by following the evolution of the longitudinal electric energy at small scales of $\mathcal{E}$ (previously reported in Figure 1 in the time interval $0 < t < 100$) up to the time $t = 400$. The results of these new simulations are shown in the top left panel of Figure 6. From this figure, we note that while for $T_e/T_p = 10$ the level of $\mathcal{E}$ is almost stable in time, for $T_e/T_p = 1, 3,$ and 6 marked low-frequency oscillations appear. Moreover, for $T_e/T_p = 1$ the electric energy definitively dissipates at $t > 340$. We also point out that the simulation for $T_e/T_p = 3$ has been extended up to $t = 500$ in order to clearly show a complete time oscillation of $\mathcal{E}$.

In order to understand the physical mechanism that drives these oscillations, we consider the case of $T_e/T_p = 1$ in detail. In particular, we look at the proton distribution function at fixed time instants during the simulation, indicated in the top right panel in Figure 6 by red diamonds superposed on the time signal of $\mathcal{E}$ at $T_e/T_p = 1$. At each time instant indicated by a red diamond, we calculate the reduced proton distribution function, defined as $f_R = \int dv_y dv_z f$; then we spatially average f_R in the interval corresponding to the trapped particle population (see, for example, the vertical dashed lines in the bottom panel of Figure 2 for the case of $T_e/T_p = 3$). The red diamonds have been located in such a way to consider the saturation phase (a), the damping phases (b) and (c), the growing phases (d) and (e), and the dissipation phase (f) in the time evolution of $\mathcal{E}$.

The velocity distributions (zoomed around the position of the proton beam) corresponding to the cases listed above are displayed in the middle and bottom panels of Figure 6, where $\langle\rangle$ indicate the spatial average and the vertical dashed lines in each plot represent the value of the phase speed of the IBk waves $v_\phi^{(\mathrm{IBk})} \simeq 0.6$. From these pictures we note that in case (a) the IBk phase velocity is located near the bottom of the well in between the principal and the secondary proton populations (a region of null velocity derivative). On the other hand, $v_\phi^{(\mathrm{IBk})}$ falls in regions of negative velocity slope in cases (b) and (c) and in regions of positive velocity slope in cases (d) and (e). This evidence suggests that the damping/growing behavior of $\mathcal{E}$ is determined by the sign of the velocity derivative of $\langle f_R \rangle$ at $v_\phi^{(\mathrm{IBk})}$, as in a typical case of a beam–plasma instability (Krall & Trivelpiece 1986).

Since the value of $v_\phi^{(\mathrm{IBk})}$ does not change with time, we conclude that the oscillating behavior of $\mathcal{E}$ is related to the longitudinal vibrations of the bulk of the proton velocity distribution: as can be seen in Figure 6, the velocity location of the proton beam remains fixed, but the core of the distribution vibrates in such a way that the velocity derivative of $\langle f_R \rangle$ calculated at $v_\phi^{(\mathrm{IBk})}$ changes sign with time. We also note that the height of the secondary proton beam changes accordingly to the time evolution of $\mathcal{E}$: the beam is more accentuated during the growth phases than during the damping phases. By a rough estimate from the top right panel of Figure 6, the characteristic oscillating time of $\mathcal{E}$ is $\simeq 60\Omega_{\mathrm{cp}}^{-1}$, approximately the period of the pump waves; this means that the longitudinal vibration of $\langle f_R \rangle$ is presumably triggered by the initial conditions of our simulations. Finally, it is worth noting that in case (f), corresponding to the dissipation phase, the secondary beam survives even though the electrostatic activity has been completely dissipated. This process of electric energy dissipation can possibly depend on the fact that the energy injected at $t = 0$ in large wavelength fluctuations is not replenished in our decay turbulence simulations.

It is worth noting that the marked oscillating time behavior of $\mathcal{E}$ at low values of T_e/T_p misled us in Valentini et al. (2008), where we erroneously claimed that for $T_e/T_p = 1$ the energy level of the electrostatic fluctuations at short scales is
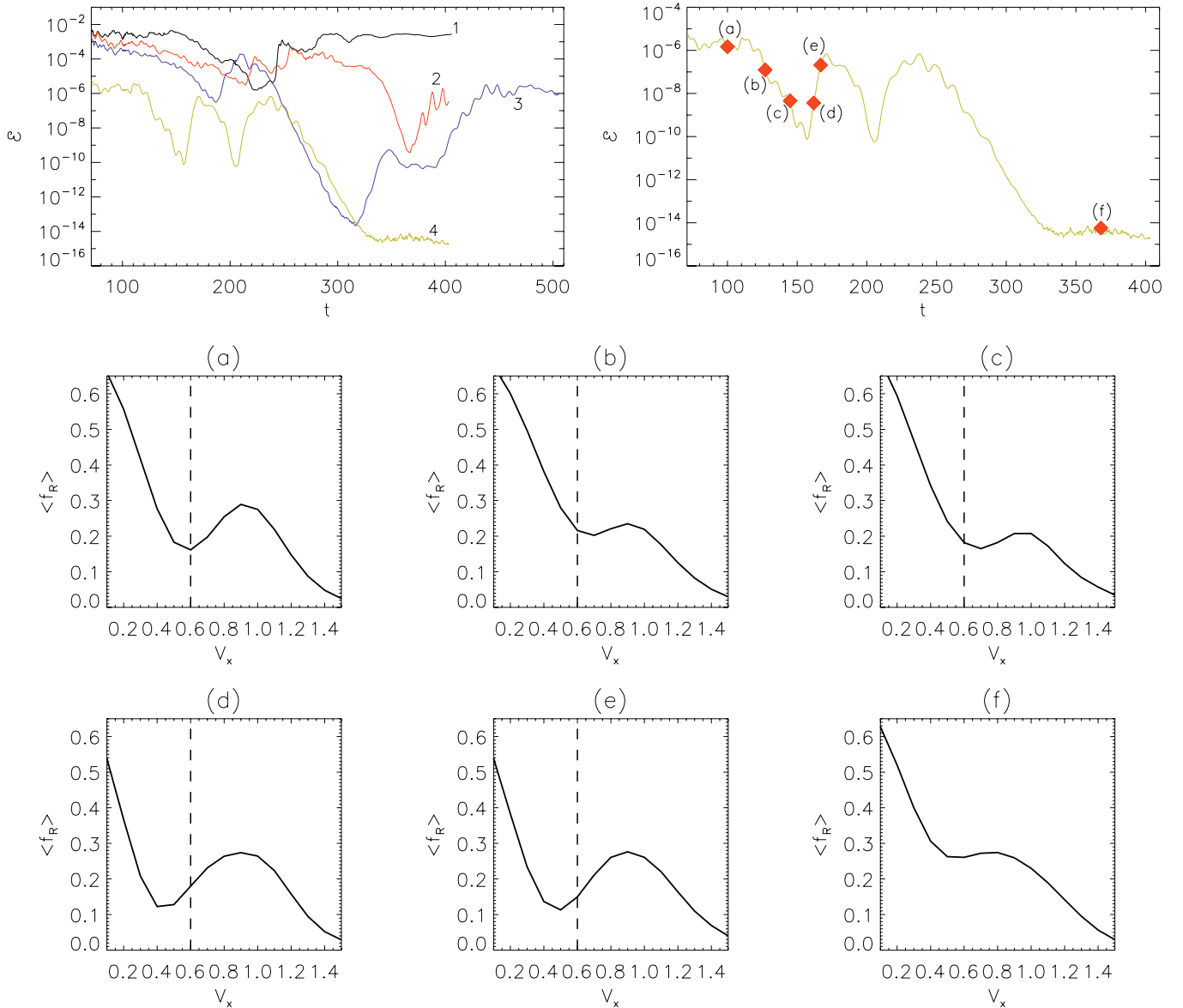
Figure 6. Top left panel: late time evolution of $\mathcal{E}$ for $T_e/T_p = 10$ (black line (1)), $T_e/T_p = 6$ (red line (2)), $T_e/T_p = 3$ (blue line (3)), and $T_e/T_p = 1$ (green line (4)). Top right panel: late time evolution of $\mathcal{E}$ for $T_e/T_p = 1$. Middle and bottom rows: velocity dependence of the spatially averaged reduced proton distribution $\langle f_R \rangle$ at the time instants indicated by the red diamonds in the top right panel; the vertical dashed lines indicate the phase speed of the IBk waves, $v_\phi^{(IBk)} \simeq 0.6$.
(A color version of this figure is available in the online journal.)

10 orders of magnitude lower than for $T_e/T_p = 10$. In fact, in Valentini et al. (2008) we had not yet realized that the electric energy oscillates with time at low values of T_e/T_p, as shown in Figure 6, and we had compared the value of $\mathcal{E}$ in the cases of $T_e/T_p = 1$ and 10 at the time instant $t = 200$, when a minimum occurs for $T_e/T_p = 1$ (see Figure 6).

As we previously said, the more the electron-to-ion temperature ratio increases, the less evident oscillations in the time evolution of $\mathcal{E}$ become (see the top left panel of Figure 6). Within the scenario of the beam–plasma instability pictured above, this evidence can be explained by taking into account that the longitudinal velocity width of the trapped particle region in the proton velocity distribution increases as T_e/T_p increases (since the amplitude of the electric oscillations is correlated to T_e/T_p, as shown in the top left panel of Figure 6). Even though the bulk of the velocity distribution vibrates, as already discussed for $T_e/T_p = 1$, for large values of T_e/T_p the IBk phase

velocity always falls in a region of nearly zero velocity slope since this region is now significantly larger than in the case of $T_e/T_p = 1$.

3. SUMMARY AND CONCLUSIONS

In this paper, we discussed the numerical results of hybrid Vlasov–Maxwell simulations of turbulence at short scale in the solar wind. The system dynamics in the tail at short wavelengths of the turbulent cascade are analyzed in terms of the electron-to-proton temperature ratio. Our numerical results show that the electrostatic activity in the termination at small spatial scale lengths of the energy spectra, also recovered in the solar-wind data from spacecraft, mainly consists of a novel branch of waves, called IBk waves, that propagate with phase speed comparable to the proton thermal velocity along the direction of the ambient

magnetic field. The peculiarity of these electrostatic fluctuations is that, at variance with the usual IA waves, they do not undergo Landau damping even at low values of the electron-to-proton temperature ratio since they are sustained by the presence of diffusive plateaus in the longitudinal proton velocity distribution. We emphasize that this numerical evidence can be of strong impact for the case of the solar-wind plasma, where the ratio between electron and proton temperature is typically of order unity.

From the analysis of the numerical results of our hybrid Vlasov–Maxwell simulations, we also found that in correspondence with the propagation of the IBk waves, the proton velocity distribution displays the generation of a field-aligned beam of accelerated particles with mean velocity close to the local Alfvén speed. We point out that the mean velocity of this beam does not depend on the electron-to-proton temperature ratio, and for β_p of order unity, the appropriate value for the case of the solar wind, it always remains close to V_A, in agreement with the experimental data from observations. We emphasize that previously proposed mechanisms (Araneda et al. 2008; Matteini et al. 2010), based on the excitation of IA fluctuations by the parametric instability of large-scale Alfvén waves, succeed in reproducing the field-aligned proton beam at $v \simeq V_A$ for a different range of plasma parameters (large T_e/T_p, low β_p, and $(T_e/T_p)\beta_p \simeq 1$).

On the other hand, the mechanism discussed in the present paper, based on the excitation of the electrostatic IBk branch, naturally works in the physical conditions of the interplanetary medium, even for small values of the electron-to-proton temperature ratio, provided that the proton plasma beta is of order unity. These numerical results describe a reliable mechanism for explaining the complex phenomenon detected in many solar-wind measurements from spacecraft and thus can be of relevant importance in the study of the evolution of solar-wind turbulence toward short wavelengths.

REFERENCES

Alexandrova, O., Saur, J., Lacombe, C., et al. 2009, Phys. Rev. Lett., 103, 165003
Araneda, J. A., Marsch, E., & Vinas, A. 2008, Phys. Rev. Lett., 100, 125003
Bale, S. D., Kellogg, P. J., Mozer, F. S., Horbury, T. S., & Reme, H. 2005, Phys. Rev. Lett., 94, 215002
Carbone, V., Malara, F., & Veltri, P. 1995, J. Geophys. Res., 100, 1763
Dobrowolny, M., Mangeney, A., & Veltri, P. 1980, A&A, 83, 26
Gurnett, D. A., & Andreson, R. R. 1977, J. Geophys. Res., 82, 632
Gurnett, D. A., & Frank, L. A. 1978, J. Geophys. Res., 83, 58
Gurnett, D. A., Marsch, E., Pilipp, W., Schwenn, R., & Rosenbauer, H. 1979, J. Geophys. Res., 84, 2029
Hellinger, P., Travncek, P., Kasper, J. C., & Lazarus, A. J. 2006, Geophys. Res. Lett., 33, L09101
Heuer, M., & Marsch, E. 2007, J. Geophys. Res., 112, A03102
Holloweg, J. V., & Isenberg, P. A. 2002, J. Geophys. Res., 107, 1147
Howes, G. G., Dorland, W., Cowley, S. C., et al. 2008, Phys. Rev. Lett., 100, 065004
Kennel, C. F., & Engelmann, F. 1966, Phys. Fluids, 9, 2377
Krall, N. A., & Trivelpiece, A. W. 1986, Principles of Plasma Physics (San Francisco, CA: San Francisco Press)
Lacombe, C., Salem, C., Mangeney, A., et al. 2002, Ann. Geophys., 20, 609
Longtin, M., & Sonnerup, B. U. O. 1986, J. Geophys. Res., 91, 6816
Mangeney, A., Salem, C., Lacombe, C., et al. 1999, Ann. Geophys., 17, 307
Marsch, E., Ao, X.-Z., & Tu, C.-Y. 2004, J. Geophys. Res., 109, A04102
Marsch, E., Muhlhauser, K.-H., Schwenn, R., et al. 1982, J. Geophys. Res., 87, 52
Matteini, L., Landi, S., Velli, M., & Hellinger, P. 2010, J. Geophys. Res., 115, A09106
Matthaeus, W. H., Goldstein, M. L., & King, J. H. 1986, J. Geophys. Res., 91, 59
Pickett, J. S., Chen, L.-J., Kahler, S. W., et al. 2004, Ann. Geophys., 22, 2515
Sahraoui, F., Goldstein, M. L., Robert, P., & Khotyaintsev, Yu. V. 2009, Phys. Rev. Lett., 102, 231102
Schwenn, R., & Marsch, E. 1991, Physics of the Inner Heliosphere II. Particles, Waves and Turbulence (Berlin: Springer)
Tu, C.-Y., Marsch, E., & Qin, Z.-R. 2004, J. Geophys. Res., 109, A05101
Valentini, F., Califano, F., Perrone, D., Pegoraro, F., & Veltri, P. 2011, Phys. Rev. Lett., 106, 165002
Valentini, F., Califano, F., & Veltri, P. 2010, Phys. Rev. Lett., 104, 205002
Valentini, F., Travnicek, P., Califano, F., Hellinger, P., & Mangeney, A. 2007, J. Comput. Phys., 225, 753
Valentini, F., & Veltri, P. 2009, Phys. Rev. Lett., 102, 225001
Valentini, F., Veltri, P., Califano, F., & Mangeney, A. 2008, Phys. Rev. Lett., 101, 025006